Optically induced quasiparticle density profiles in superconducting thin films

N. E. Glass and D. Rogovin
Rockwell Science Center, 1049 Camino Dos Rios, Thousand Oaks, California 91360
(Received 8 July 1991)

We present numerical solutions of the coupled phonon-quasiparticle rate equations, with quasiparticle (qp) and phonon diffusion included, for a superconducting thin film illuminated by a temporally pulsed and spatially inhomogeneous optical intensity pattern. We consider optical intensities in the form of both a finite circular spot with a Gaussian cross section and a sinusoidal interference pattern. Thereby we demonstrate that spatially well-defined qp density profiles, including a qp grating, can be optically induced on nanosecond time scales. For the qp grating we use the T^* formalism to calculate the resulting conductivity grating in the film, and then calculate the grating diffraction peaks for incident microwaves.

I. INTRODUCTION

The possibility of using laser interference patterns to "write" spatial information in a medium by modulating the dielectric constant is a central idea in much of modern nonlinear optics. In particular, optical index gratings, the radiation-induced periodic spatial variations in an active medium's dielectric constant, are responsible for numerous active optical processes, such as phase conjugation, and are of enormous interest in nonlinear optics.[1] To date, research has focused on laser-induced spatial structures that control infrared and visible wavelength radiation using such nonlinear materials as atomic vapors, photorefractives, optical Kerr media, semiconductors, and liquid crystals. In this paper we discuss an extension of the basic ideas of this field to superconducting thin films. We show how optical illumination can spatially modulate a superconductor's quasiparticle (qp) density and thereby modulate its complex conductivity, thus causing it to diffract microwaves. Optical illumination can create gratings that not only diffract but can also couple microwaves to guided waves in a dielectric substrate supporting the film. In addition to the technological applications of using lasers to thus modulate microwaves spatially and temporally, such interactions may be measured to learn more about the underlying qp dynamics in nonequilibrium superconductors.

The theory presented here predicts that well-defined quasiparticle spatial structures can be created in thin-film superconductors with a laser interference pattern by using, for example, two degenerate laser beams that coherently interfere with one another. The presence of laser light gives rise to pair splitting that generates quasiparticle population distributions (for example, gratings) in accordance with the optical intensity pattern.[2,3] These qp spatial structures, in turn, establish conductivity variations within the superconductor, which are active below the pair-splitting frequency, i.e., at microwave frequencies. Since the conductivity variations are in both the real and imaginary parts, both phase and amplitude index modulations are established. We examine the steady-state and transient dynamics of these structures and show that they form quite rapidly, on the order of 0.5 ns for Nb thin films. In particular, we demonstrate that the existence of periodic qp structures can be verified by measuring the angle-resolved transmittance and reflectance of diffracted microwaves [or, more specifically, millimeter (mm) waves]. We have calculated that well-defined off-specular peaks appear, corresponding to the grating diffraction orders. These peaks are greatly enhanced when the mm waves are coupled via a prism into the guided wave modes that exist within a dielectric substrate supporting the superconducting film. The peaks can be directly traced to the presence of the optical index gratings: in the absence of the laser beams no gratings are created within the superconducting film, and all of the prism-coupled guided-wave energy is absorbed or is reradiated in the specularly reflected direction.

The basic physics underlying the optically induced formation of index variations in superconducting thin films is as follows. When light irradiates a superconductor, pair splitting generates qp's, which are excited to high-lying states, since optical frequencies are much higher than the energy gap (Δ). Within a few picoseconds, the qp fall to the bottom of the conduction band (in a phonon avalanche) where they eventually undergo recombination to form Cooper pairs accompanied by phonon emission.[4,5] For situations of interest to us, the superconducting thin film is irradiated by laser beams that form an interference pattern. In regions where there is coherent interference, the light intensity will be high and numerous Cooper pairs will be split. In these regions, the qp and phonon densities will be noticeably larger than their equilibrium values and the effective electronic temperature will be high. In regions where the beams interfere destructively, few qp will be created and the qp and phonon densities will be close to their thermal equilibrium values. Here, the effective electronic temperature will be close to that of the thermal bath that is in contact with the thin films. Thus, the effective electronic temperature will be spatially dependent in accord with the laser interference pattern. Furthermore, the presence of a qp spatial pattern implies the existence of a spatial modulation of the conductivity for $\hbar\omega < 2\Delta$. The qp and phonon diffusion processes will smear out this spatial modulation, so that

the quasiparticle, temperature, and conductivity patterns will not be identical with the light interference pattern.

We review the basic model in Sec. II, and then in Sec. III we present numerical results for the qp spatial and temporal responses to two different optical intensity patterns. First, we explore the response to light illuminating the superconducting film in a finite circular spot with a Gaussian cross section. This allows us to examine the diffusion of qp's, from light to dark regions, as a function of time. Second, we present our results for the response to a sinusoidal intensity pattern, namely, the formation of qp gratings. We then discuss the electrodynamics of these qp gratings: we present our calculations for the resultant conductivity gratings and the grating-diffraction peaks of incident microwaves. We conclude the discussion in Sec. IV.

II. MODEL

When the laser pulse width is long compared to the time needed for the qp to fall to the bottom of the conduction band, the kinetics of quasiparticle and phonon creation and decay are well described by the Rothwarf-Taylor rate equations.[6] In the scheme developed by Parker[7] (and later extended to transient, spatially inhomogeneous, driving fields[2,3]), the qp and phonons establish a new equilibrium distinguished by an effective temperature T^*, which is obtained from the qp density via the BCS gap equation. Thus, to find the effective temperature $T^*(\mathbf{r},t)$ as a function of position $\mathbf{r}$ and time t, we solve first the coupled Rothwarf-Taylor equations (with diffusion terms added) for the qp and phonon density, $n_{\rm qp}(\mathbf{r},t)$ and $n_{\rm ph}(\mathbf{r},t)$.[3] Specifically, we solve for $u=n_{\rm qp}/n^0_{\rm qp}$ and $v=n_{\rm ph}/n^0_{\rm ph}$, where the superscripts 0 signify the qp equilibrium and the phonon density associated with the thermal reservoir. These equations take the dimensionless form

$$\frac{\partial}{\partial \mathcal{T}}u=(1+b)^{-1}Q(\tilde{\mathbf{r}},\mathcal{T})-u^2+v+\tilde{\nabla}^2u\ , \tag{1a}$$

$$\frac{\partial}{\partial \mathcal{T}}v=\frac{\tau^0_R}{\tau_{\rm es}}\left[1+bu^2-(1+b)v+(1+b)\left[\frac{L_{\rm ph}}{L^0_{\rm qp}}\right]^2\tilde{\nabla}^2v\right]\ . \tag{1b}$$

In Eqs. (1), τ^0_R is the equilibrium qp recombination time, in terms of which we define the dimensionless time variable $\mathcal{T}=t/\tau^0_R$ and a qp diffusion length $L^0_{\rm qp}=(D_{\rm qp}\tau^0_R)^{1/2}$, which in turn defines the position variable $\tilde{\mathbf{r}}=\mathbf{r}/L^0_{\rm qp}$ and $\tilde{\nabla}=L^0_{\rm qp}\nabla$. The length scale for the phonons is set by $L_{\rm ph}=(D_{\rm ph}\tau_{\rm ph})^{1/2}$, where the phonon lifetime is $\tau_{\rm ph}=\tau_{\rm es}\tau_B/(\tau_{\rm es}+\tau_B)$. Here $D_{\rm qp[ph]}$ is the qp (phonon) diffusion coefficient (of order $v_f^2\tau^0_R$ $[v^2_{\rm ph}\tau_{\rm ph}]$ in terms of the Fermi and phonon velocities); τ_B is the pair-breaking time; $\tau_{\rm es}$ is the phonon escape time to the thermal reservoir. In Eqs. (1), $b=\tau_{\rm es}/\tau_B$. In deriving Eqs. (1), the result of the condition for detailed balance, $2\tau^0_R/\tau_B=n^0_{\rm qp}/n^0_{\rm ph}$, was employed. Finally, Q is a dimensionless drive current

$$Q=\tilde{\tau}^0_R[I_{\rm qp}+I_{\rm ph}2b/(1+b)]/n^0_{\rm qp}\ .$$

Here, $I_{\rm qp}(I_{\rm ph})$ is the laser-field-induced qp (ph) creation rate per unit volume, and $\tilde{\tau}^0_R=\tau^0_R(1+b)$. The validity of the T^* model requires that $\tau_{\rm es}/\tau_B\gg1$ (Ref. 8), in which case, it does not matter whether we consider the laser as indirectly producing a phonon current (from the phonon avalance) or (as in Refs. 2, 3, 7, and the present work) we take $I_{\rm ph}=0$ and $I_{\rm qp}=P/(V\Delta)$, where the volume V absorbs laser power P, all of which is assumed to create qp's.

We have carried out numerical solutions to the coupled, partial, differential equations of Eq. (1), for the case in which the optically induced drive current is a square pulse in time (on at $t=0$ and off at $t=t_c$) and for two distinct spatial patterns, a circular spot with a Gaussian profile and a sinusoidal grating.

Reference 3 showed that after a sudden switching on of a laser pulse, the rise time to steady state for the qp is $\tilde{\tau}_R=\tilde{\tau}^0_R/(1+Q)^{1/2}$. For the numerical work presented in the next section, we have thus taken the temporal pulse width of the optical drive to be $t_c=5\tilde{\tau}_R$ to assure that the system has virtually attained steady state before the laser is switched off.

As for the spatial dependence, we considered first the case in which the optical illumination falls within a circular spot on the plane of the film, its intensity depending only the radial coordinate $\rho=(x^2+y^2)^{1/2}$, the distance from the spot center (independent of z, the direction normal to the film surface, and of the angle about z). Then in Eq. (1)

$$\tilde{\nabla}^2=\frac{1}{\tilde{\rho}}\frac{\partial}{\partial\tilde{\rho}}\tilde{\rho}\frac{\partial}{\partial\tilde{\rho}}\ ,$$

where $\tilde{\rho}=\rho/L^0_{\rm qp}$. Specifically, we have investigated an intensity profile with a radial falloff that is Gaussian with a finite cutoff distance. Thus we have

$$\begin{aligned}Q(\mathbf{r},t)&=Q(\rho,t)\\&=Q_0\Theta(t_c-t)\Theta(t)\Theta(\rho_c-\rho)\exp(-\rho^2/2\delta^2)\ .\end{aligned} \tag{2}$$

Here, the Θ functions (Heaviside functions) represent the temporal pulse of width t_c and the spatial cutoff at ρ_c. The finite spatial extent of the spot allows us to study qp diffusion out of the illuminated region and thus to estimate in general terms the effects of qp diffusion on the smearing out of induced qp spatial profiles.

Secondly, we considered a one-dimensional grating, where the pulsed laser interference pattern gives rise to a space and time dependent $I_{\rm qp}$, which in Q becomes

$$Q(x,t)=[Q_0+\Delta Q\cos(2\pi x/a)]\Theta(t_c-t)\Theta(t)\ , \tag{3}$$

where a is the spatial period and t_c is again the temporal pulse width.

In the work presented here, the laser-induced length scales (δ for the Gaussian spot and a for the grating) are taken to be on the order of millimeters, since we propose probing the optically created qp structures with electromagnetic (EM) radiation of millimeter (mm) wavelengths. Such wavelengths correspond to probe frequencies ν close to but less than the pair-splitting frequency. Thus, the length scales for the induced qp patterns will be

much larger than the length scales associated with any possible phase transitions to the multigap states that may occur in nonequilibrium superconductors—transitions that are not described in the T^* formalism.[9] A reasonable assumption is that for moderate driving forces and ambient temperatures (here $T/T_c=0.5$ and $T^*/T_c \leq 0.8$), these spontaneous inhomogeneities can be avoided, and even if they are present, their spatial scale is small enough that they will not measurably influence the mm wave probe of the laser-induced grating.

Once we have the solution for the qp density, $n_{qp}(\rho,t)$ or $n_{qp}(x,t)$, then we find the corresponding T^* by applying a generalization of Parker's technique (as described in Ref. 3). The qp density at each point in space and time is used to obtain the effective quasiparticle temperature $T^*(\mathbf{r},t)$ by using the BCS expression for n_{qp} (in terms of the BCS density of states) and the BCS gap equation. The electronic distribution function is assumed to be a Fermi-Dirac function, but characterized by T^*. This distribution function is then used in conjunction with the Mattis-Bardeen[10] expression for the real and imaginary parts of the conductivity, σ_1 and σ_2. We are justified in using a local theory of the electrodynamics, since the spatial scale for the changing electromagnetic field parallel to the film's surface, set by the Gaussian δ or the grating period a, is much greater than any length scale (e.g., the coherence length) of the superconductor.

III. NUMERICAL RESULTS

We now present results for the time evolution and the spatial dependence of the qp density and the microwave conductivity σ, which are induced by the two different driving-optical-intensity patterns just discussed. The numerical solutions make use of the method of lines with cubic Hermite polynomials.

The numerical work was carried out for a film of Nb, of thickness d, in contact with a reservoir whose temperature is maintained at $T=0.5T_c$. The important phonon trapping factor $(1+b)$ requires the value of $b=\tau_{es}/\tau_B$, which can be estimated from the expression[11]

$$\tau_{es}/\tau_B=(4d/\eta\nu_{ph})/\tau_B \ , \tag{4}$$

where the phonon coupling factor η^{-1} goes from 1 to 100, so that τ_{es}/τ_B goes approximately from 20 to 2000 for a 0.1-μm film or from 1 to 100 for a 50-Å film. We have chosen values of τ_{es}/τ_B of 20, 60, and 500.

For qp's of energy equal to $\Delta(T)$ and for $T=0.5T_c$, the equilibrium recombination time τ_R^0 is $\cong 1.02\tau_0=0.152$ ns (calculated according to Ref. 12, where τ_0 is a characteristic time given in Table I of Ref. 11). Then the phonon-enhanced recombination time, in the absence of laser illumination, $\tilde{\tau}_R^0$ is 3.18 ns, 9.25 ns, and 76 ns, respectively, for $\tau_{es}/\tau_B=20$, 60, and 500.

Values for Q_0 [see Eqs. (2) and (3)] of 30.42, 60.84, and 725.87 were employed. Corresponding to $Q=Q_0$ there are a qp current $I_{0_{qp}}$ and a laser power absorbed by the film P_0, according to the relation

$$Q_0=(1+\tau_{es}/\tau_B)\frac{\tau_R^0}{n_{qp}^0}\frac{P_0}{\Delta(T)Ad'} \ ,$$

where the volume V absorbing the optical energy (all of which is assumed to go into creating qp's or phonons of energy 2Δ) is expressed as the area A of illumination times the depth d'. Here d' is either the skin depth (say 350 Å) or the film thickness d whichever is smaller. The exact integral over the density of states gives $n_{qp}^0=3.23\times10^{18}$ cm^{-3}, and from the BCS gap equation $\Delta(T)=1.478$ meV, while the peak power flux per unit area or peak optical intensity is $P_0/A=S_0$. Then for $d>$ skin depth, we obtain for S_0, in W/cm^2,

$$S_0=17.66Q_0/(1+\tau_{es}/\tau_B) \ , \tag{5a}$$

so that for $Q_0=30.42$, we have $S_0=25.6$, 8.81, and 1.07 W/cm^2 for $\tau_{es}/\tau_B=20$, 60, and 500, respectively. For $d<$ skin depth,

$$S_0=5.045\times10^6Q_0d/(1+\tau_{es}/\tau_B) \ , \tag{5b}$$

so that for $Q_0=30.42$ and $d=50$ Å, we have $S_0=3.65$, 1.26 and 0.153 W/cm^2 for $b=20$, 60, and 500.

The recombination time $\bar{\tau}_R$ (which is also the rise time to steady state under a constant driving field characterized by Q) that here corresponds to the $Q=Q_0=30.44$ is 0.568 ns, 1.65 ns, and 13.6 ns for $b=20$, 60, and 500.

Corresponding to the time scales τ_R^0, $\tilde{\tau}_R^0$, and $\bar{\tau}_R$ there are the following length scales for qp diffusion. Without phonon trapping and at equilibrium, $L_{qp}^0=(1/3)^{1/2}v_F\tau_R^0=0.012$ cm. With phonon trapping and $\tau_{es}/\tau_B=20$, 60, and 500, we have (1) at equilibrium, $\tilde{L}_{qp}^0=(1/3)^{1/2}v_F\tilde{\tau}_R^0=0.25$, 0.73, and 6.0 cm and (2) at steady state under the illumination of $Q_0=30.42$, $\tilde{L}_{qp}=(1/3)^{1/2}v_F\bar{\tau}_R=0.045$, 0.13, and 1.07 cm.

A. The circular spot with Gaussian profile

We have solved the coupled partial differential equations of Eqs. (1) with the driving force Q given by Eq. (2). The initial conditions are $u(\rho,t=0)=v(\rho,t=0)=0$. There are two boundary conditions, the first of which is

$$\left[\frac{\partial}{\partial\rho}u\right]_{\rho=\rho_0}=\left[\frac{\partial}{\partial\rho}v\right]_{\rho=\rho_0}=0 \ .$$

Here ρ_0 ($\gg\rho_c$, the laser cutoff) is an arbitrary point where the currents ($\mathbf{J}=-D\nabla n=-\hat{\rho}D\partial n/\partial\rho$) are said to vanish and which is set simply by choosing larger and larger values until the solutions change by less than a specified amount. The second boundary condition is

$$\left[\frac{\partial}{\partial\rho}u\right]_{\rho=0}=\left[\frac{\partial}{\partial\rho}v\right]_{\rho=0}=0 \ ,$$

as required by symmetry, since ∇u (or ∇v) $[=\hat{\rho}\partial/\partial\rho(u$ or $v)]=0$ at the origin (also, a nonzero derivative at the origin would imply the presence of a δ-function-like point source at the origin, which does not exist here). We have, moreover, from L'Hôpital's rule

$$\lim_{\rho\to 0} \nabla^2(u \text{ or } v) = 2\partial^2/\partial\rho^2(u \text{ or } v) .$$

We solved the coupled partial differential equations, Eqs. (1), under the assumption that the laser is switched on at $t=0$ and off at $5\tilde{\tau}_R$ and that the laser spot size is determined by a cutoff distance of $\rho_c = 6L^0_{qp} = 0.072$ cm. The Gaussian power falloff within the spot is determined by $\delta = 2.77L^0_{qp}$.

Figure 1(a), for $\tau_{es}/\tau_B = 20$ and $Q_0 = 30.42$, shows the time evolution of the qp density n_{qp} at five different points in space, i.e., at five distances from the beam center. By the time of the beam switchoff t_c the density n_{qp} inside the spot has essentially reached a constant, steady-state, value. This steady-state density is less than the steady-state value for the case of uniform illumination for the same Q. For example, at $\rho=0$ and $t=t_c$ (where $Q=Q_0$), we have $n_{qp}/n^0_{qp} \simeq 4.5$ as compared to $n^{ss}_{qp}/n^0_{qp} = (1+Q_0)^{1/2} = 5.6$ under *uniform* steady-state (ss) illumination (Ref. 3). The reduction in n_{qp} is due to qp diffusion from high- to low-density regions, and, hence, from within the illuminated spot to outside it. The curves labeled $\rho/L^0_{qp} = 9$ and 12 are for points outside the spot. Here we see that n_{qp} continues to grow for a while after the time of the beam shutoff, due to the diffusion of qp's from inside to outside the spot. Figure 1(b) shows n_{qp} as a function of distance at five times: the curves labeled $t/\tilde{\tau}_R = 0.5$ and 2.5 are at $t < t_c$; the curve $t/\tilde{\tau}_R = 5$ is at t_c when the system has nearly attained its steady-state condition; and $t/\tilde{\tau}_R = 6.5$ and 9 are for $t > t_c$, i.e., after the beam shutoff. For times $t > t_c$, the figure shows the qp density decaying toward its equilibrium value as the qp's recombine and diffuse. The figure also shows the shape of the distribution changing from near Gaussian, for $t < t_c$, when it closely follows the laser illumination pattern, to nearly a flat line for $t > t_c$ as the qp's diffuse from the center toward the tail of the distribution.

We now consider what happens if we increase $b = \tau_{es}/\tau_B$ [for example, by using thicker films—bigger d—or slower heat transfer—smaller η, as in Eq. (4)], while keeping Q constant ($Q_0 = 30.42$). From Eq. (5a) we see that this situation means that the optical intensity S is being lowered as b is increased [if we are changing d to change τ_{es}, then we must have $d >$ skin depth for Eq. (5a) to apply and for the above statement to hold]. Under these conditions, since Q remains constant, the qp density that would correspond to the steady state under constant uniform illumination remains the same, $n^{ss}_{qp}/n^0_{qp} = (1+Q)^{1/2}$. This constancy of the qp density occurs even though we are decreasing the input power and photon flux that produce the qp's, since this decrease is compensated by the phonons' remaining in the film a longer time to split more pairs. This compensation is seen in Figs. 2 and 3 for the cutoff Gaussian beam as b increases from 20 to 60 to 500, under constant Q_0. As b increases, the value of n_{qp} (for every time step) becomes smaller at and near the spot' center, $\rho=0$, but it becomes larger in the tail of the distribution ($\rho > \rho_c$). The lower photon flux creates fewer qp's, but the longer phonon escapetime (lifetime) yields more qp's. The latter phenomenon in-

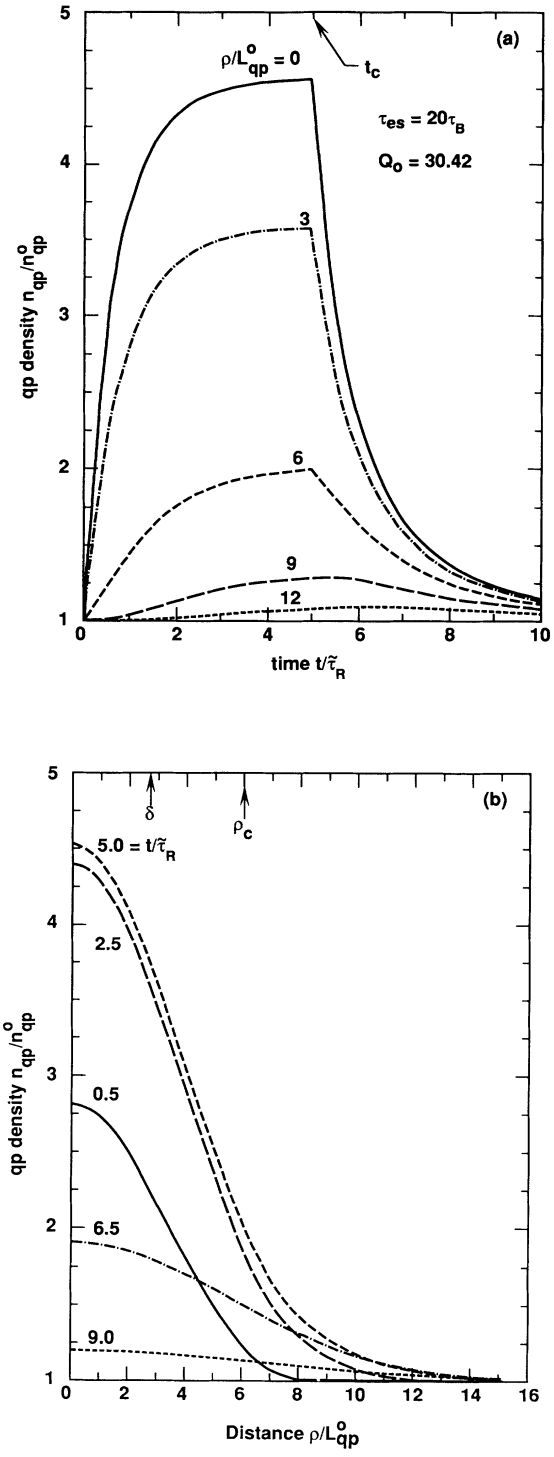

FIG. 1. Quasiparticle density normalized to its equilibrium value, for Nb film at $T=0.5T_c$ with $\tau_{es}=20\tau_B$. In response to an optical pulse (cutoff at $t_c=5\tilde{\tau}_R$) in a circular beam with a Gaussian profile ($\delta=2.77L^0_{qp}$ and cutoff at $\rho_c=6L^0_{qp}$) and a driving amplitude $Q_0=30.42$. (a) As function of time normalized to the rise time $\tilde{\tau}_R$, at five positions $\rho/L^0_{qp}=0$, 3, 6 (cutoff point), 9, and 12. (b) As function of position (radial distance ρ) normalized to the equilibrium diffusion-length L^0_{qp}, at five times $t/\tilde{\tau}_R=0.5$, 2.5, 5 (cutoff time), 6.5, and 9.

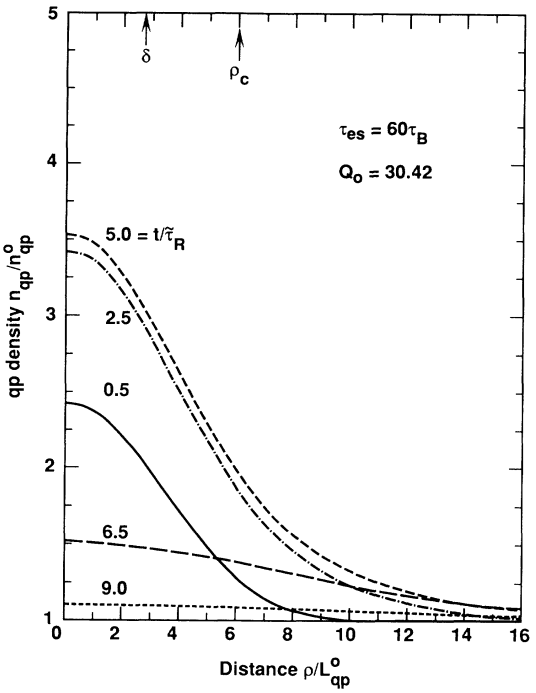

FIG. 2. Same as Fig. 1(b) except that $\tau_{es}/\tau_B = 60$.

creases the effective qp lifetimes $\tilde{\tau}_R^0$ and $\tilde{\tau}_R$ and thus increases the qp diffusion lengths $\tilde{L}_{qp}^0$ and $\tilde{L}_{qp}$ (see the values given above). The increase in qp lifetime, and accompanying increase in diffusion length, explain why on going from Fig. 1 to 2 to 3 we see the qp distribution become broader (lower in the center and higher in the tail).

Next we examine our results for the case in which τ_{es}/τ_B is increased, while the laser intensity S is held constant. From Eq. (5), we see that this means that Q (and Q_0) is being raised as τ_{es}/τ_B is raised. Now the photon flux stays constant and so does its production of qp's, while at the same time the phonons are living longer, splitting more pairs, and increasing the effective life and diffusion length of the qp's. The steady-state density under uniform illumination thus increases [as $(1+Q)^{1/2}$]. For the case in which $\tau_{es}/\tau_B = 500$ and $Q = 725.9$, we have $n_{qp}^{ss}/n_{qp}^0 = 27$ under uniform illumination, and we have $n_{qp}(\rho,t)$ as depicted in Fig. 4 for the time-pulsed Gaussian beam. The peak laser intensity by Eq. (5a) is then $S_0 = 25.6$ W/cm^2, exactly the same as when $\tau_{es}/\tau_B = 20$ and $Q_0 = 30.42$ in Fig. 1. Comparing Figs. 1 and 4, we see that the qp density is higher in Fig. 4 for all time steps and all positions, as expected—due to the longer effective qp lifetimes. On the other hand, the value of n_{qp} at $\rho = 0$ and $t = t_c$ (near its steady-state value) is a larger fraction of the spatially *uniform* steady-state value for the case in Fig. 1 [$n_{qp}(0,t_c)/n_{qp}^{ss} = 0.8$] than in Fig. 4 [$n_{qp}(0,t_c)/n_{qp}^{ss} = 0.46$]. The ratio of the qp density at $\rho = 8L_{qp}^0$ to that at $\rho = 0$ (at $t = t_c$) is larger in Fig. 4 than in Fig. 1—0.36 versus 0.32. Therefore, while n_{qp} is everywhere greater in Fig. 4 than in Fig. 1, the distributions in Fig. 4 compared to those in Fig. 1 show relatively more qp's having drifted from the spot center to the tail due to the effect of the longer qp diffusion length (between Fig. 1 and 4, $\tilde{L}_{qp}^0$ changes from $21L_{qp}^0$ to $501L_{qp}^0$, and $\tilde{L}_{qp}$ changes from $3.75L_{qp}^0$ to $18.6L_{qp}^0$). Thus, if we keep the laser intensity constant and we increase τ_{es}/τ_B, we increase the overall qp density, but we get relatively more smearing of the qp distribution due to diffusion.

Finally, since we are solving Eqs. (1) simultaneously for

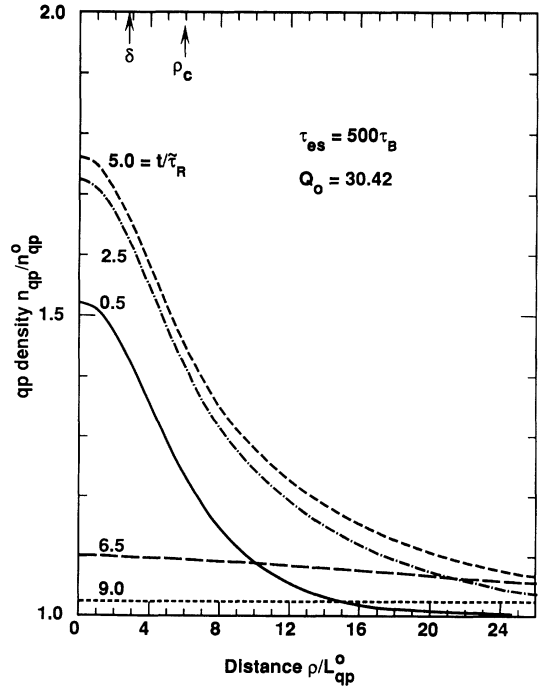

FIG. 3. Same as Fig. 1(b) except that $\tau_{es}/\tau_B = 500$.

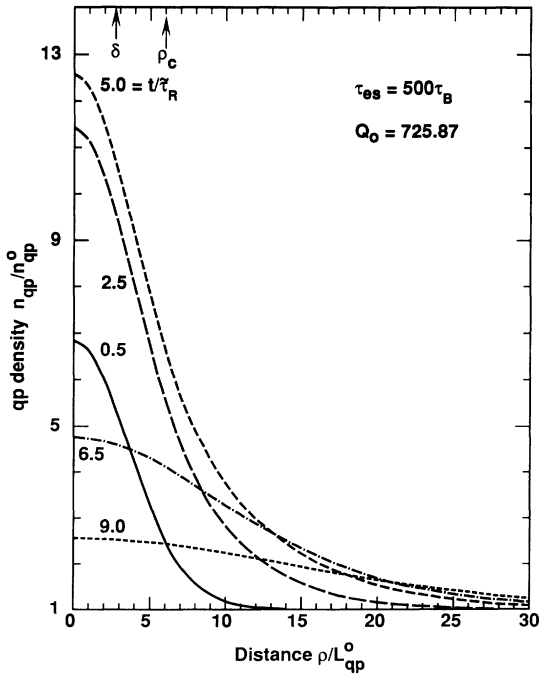

FIG. 4. Same as Fig. 1(b) except that $\tau_{es}/\tau_B = 500$ and $Q_0 = 725.87$.

the qp and phonon density, for the sake of completeness we illustrate a solution for the phonons in Fig. 5. Figure 5 for the phonons represents the same system—in fact, the same numerical simultaneous solution—as Fig. 1 for the qp's.

In Ref. 3 we introduced an approximation scheme for solving Eq. (1) by eliminating the phonon variable from the qp equation, under the assumption that the phonons adiabatically follow the qp's. This process leaves a single differential equation for the qp's and an algebraic equation for the phonons in terms of the qp density. If we use the condition for detailed balance in that algebraic equation [Eq. (2.17b) of Ref. 3], together with $I_{\rm ph}=0$, we obtain the expression

$$\frac{n_{\rm ph}}{n^0_{\rm ph}}=\left[1+\left[\frac{n_{\rm qp}}{n^0_{\rm qp}}\right]^2\frac{\tau_{\rm es}}{\tau_B}\right](1+\tau_{\rm es}/\tau_B)^{-1}\ . \tag{6}$$

Comparing this approximate expression to the exact numerical results obtained from solving the coupled differential equations simultaneously (Figs. 1 and 5), we find excellent agreement.

B. One-dimensional sinusoidal grating

Next, we solved the coupled partial differential equations for the qp's and phonons for the case in which the laser interference pattern, which drives the system, is sinusoidal along one direction in the plane of the film, represented by the $Q(x,t)$ in Eq. (3). Again we have a Nb film at $T=0.5T_c$. We chose the spatial period $a=0.2$ cm. This period is of the correct order of magnitude to diffract mm waves, and, furthermore, is long enough to prevent diffusion from washing out the induced qp grating ($a=16.6L^0_{\rm qp}$), while being short enough so that 40–60 grid points in the equation solver yield convergence. Again, the optical pulse is turned on at $t=0$ and off at $t=t_c=5\tilde{\tau}_R$.

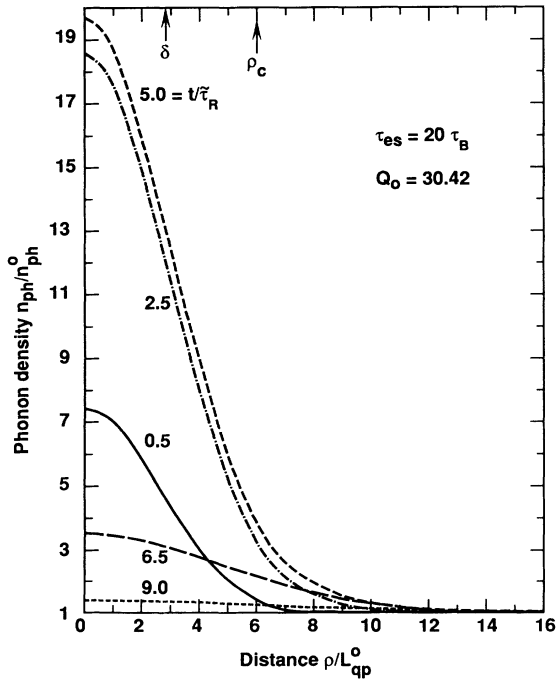

FIG. 5. Phonon density normalized to the equilibrium value of the thermal reservoir. The same system as in Fig. 1. As a function of position, at five time steps, the same as in Fig. 1(b).

To begin, we let $\Delta Q=0.1Q_0$, which defines a low grating contrast (peak-to-valley intensity difference), and with $Q_0=30.42$, we let $\tau_{\rm es}/\tau_B$ increase from 20 [Fig. 6(a)] to 500 [Fig. 6(b)]. This situation is analogous to what we did for the Gaussian beam, in going from Fig. 1 to 3. Increasing $\tau_{\rm es}/\tau_B$ with Q fixed means decreasing the laser intensity (as described above), and thus decreasing the qp production by incident photons, while the increased phonon lifetime simultaneously increases pair breaking by phonons. Thus we see little change in the total qp density in passing from Fig. 6(a) to 6(b); in 6(b) there are fewer qp's in the high-intensity areas and more in the low-intensity areas due to the increased qp diffusion lengths $\tilde{L}^0_{\rm qp}$ and $\tilde{L}_{\rm qp}$. We therefore get lower contrast qp gratings in this manner. Now on going from Fig. 6(a) to 6(c), we keep the optical power S constant by changing Q_0 from 30.42 to 725.9 as we change $\tau_{\rm es}/\tau_B$ from 20 to 500 (analogous to Figs. 1 and 4 for the Gaussian beam). The constant input power combined with the increased phonon lifetimes and the consequent increased pair splitting mean that there is a much higher overall qp density in Fig. 6(c). The contrast, however, is reduced due to the increased qp diffusion lengths.

To increase the contrast of the qp grating we returned to $\tau_{\rm es}/\tau_B=20$ and $Q_0=30.42$, and now we increased the optical contrast by letting $\Delta Q=Q_0$. The solution depicted in Fig. 7 reveals that the qp density exhibits a well-defined periodic grating structure that achieves a maximum value of nearly $7.5n^0_{\rm qp}$ at the time that the laser is switched off. Even after a single $\tilde{\tau}_R$, i.e., 0.5 ns after the laser is turned on, a significant qp grating is generated. After the laser pulse is switched off, the grating is seen to decay rapidly by qp recombination and thermal diffusion. As with each of the gratings (Figs. 6 and 7), by the time $t=9\tilde{\tau}_R$, the grating no longer exists.

We point out that this analysis is for a stationary grating. In a real experiment, the laser interference pattern—even when created with a single laser line—will have nonstationary components of the form $\cos^2(2\pi x/a-2\pi t\Delta\nu)$ corresponding to a grating velocity of $a\Delta\nu$, due to the finite linewidth $\Delta\nu$. Such a grating will still appear to be stationary on the time scales of interest as long as the time required for its motion to smear out the grating pattern, $\delta t=1/4\Delta\nu$, is much greater than the grating formation time, which as we have already noted is given by $\tilde{\tau}_R$. We thus require that $\Delta\nu<1/\tilde{\tau}_R$, and, since $\tilde{\tau}_R$ is on the order of nanoseconds, we require approximately that $\Delta\nu<10^9$ Hz. This linewidth for a laser of 1-μm wavelength is well within experimental limits.

C. Conductivity gratings and microwave diffraction

Now, we discuss the millimeter wave electrodynamics of this qp grating in a superconducting Nb film. The presence of a qp grating implies the existence of both

phase and amplitude conductivity gratings, viz., both the real and imaginary parts of the complex conductivity follow the periodic spatial modulations of the qp structure. We find the complex conductivity as described in Sec II; for each point in time and space we use $n_{qp}(x,t)$ to find the effective temperature T^* and then use the Mattis-Bardeen equations to find $\sigma(x,t)=\sigma_1(x,t)-i\sigma_2(x,t)$.

Corresponding to the qp grating depicted in Fig. 7, the results for the fractional changes in conductivity, $\Delta\sigma_1(x,t)/\sigma_1$ and $\Delta\sigma_2(x,t)/\sigma_2$ are shown in Fig. 8, at the frequency of $\nu=357.4$ GHz ($=\Delta/h$). Here, the changes $\Delta\sigma_i$ are between the initial equilibrium values σ_i and the

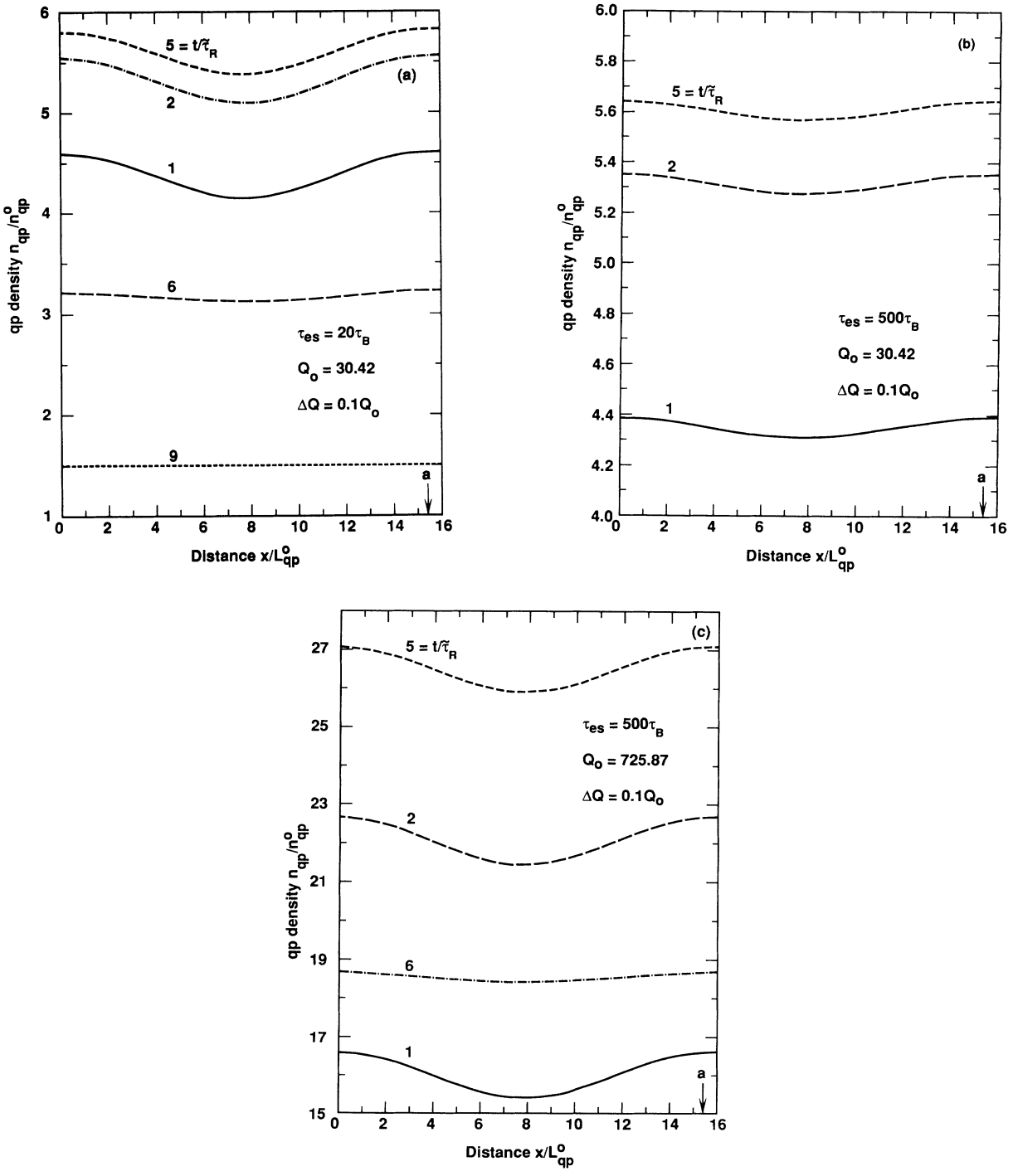

FIG. 6. Quasiparticle density normalized to its equilibrium value, for Nb film at $T=0.5T_c$. In response to an optical pulse (cutoff at $t_c=5\tilde{\tau}_R$) in a sinusoidal interference pattern (period $a=0.2$ cm). The optical intensity and resulting driving current have modulation amplitudes (ΔQ) equal to 0.1 times their average (Q_0). Plotted as a function of position x, normalized to L^0_{qp}, at five times $t/\tilde{\tau}_R=1$, 2, 5 (cutoff time), 6, and 9. (a) $\tau_{es}=20\tau_B$ and $Q_0=30.42$. (b) $\tau_{es}=500\tau_B$ and $Q_0=30.42$. (c) $\tau_{es}=500\tau_B$ and $Q_0=725.87$.

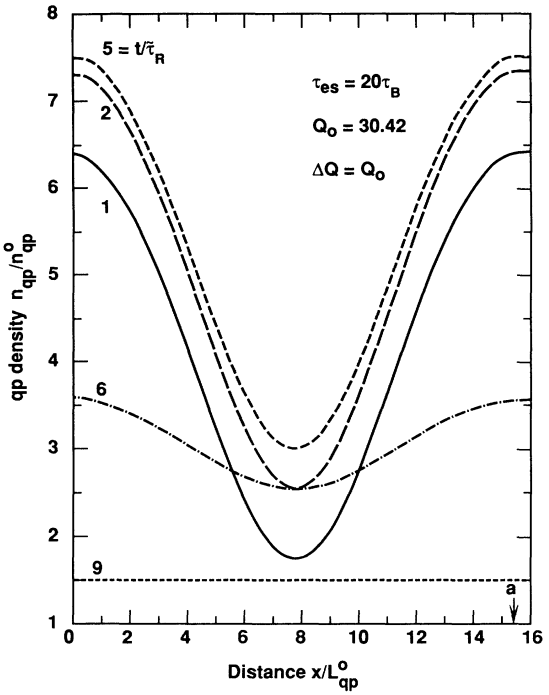

FIG. 7. Same as Fig 6(a) except that $\Delta Q = Q_0$.

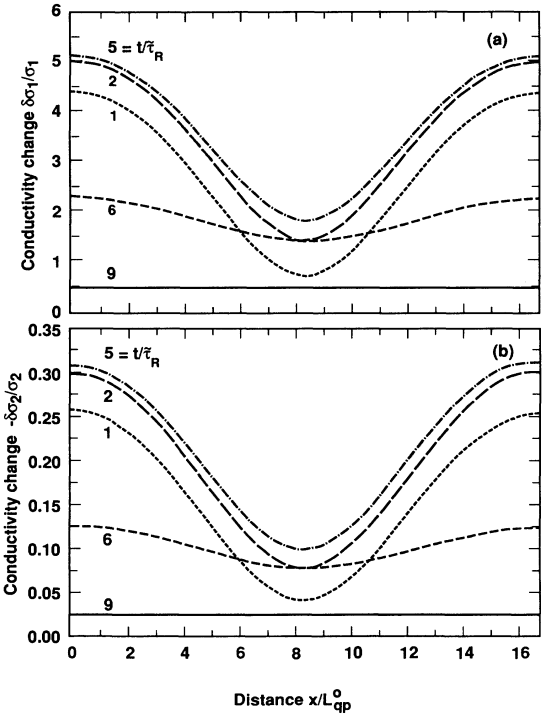

FIG. 8. The real (a) and imaginary (b) parts of the conductivity grating, at $\nu = 357.4$ GHz, as functions of position for five different times. Induced by the same sinusoidal optical interference pattern ($a = 0.2$ cm, $Q_0 = \Delta Q = 30.42$) and for the same superconductivity film (Nb at $T/T_c = 0.5$ with $\tau_{es}/\tau_B = 20$) as produced the qp grating in Fig. 7.

values under laser illumination, $\sigma_i^*(x,t)$. The conductivity gratings display the same overall spatial and temporal behavior as the qp grating. We see from these figures that the in-phase conductivity grating $[\Delta\sigma_1(x,t)/\sigma_1]$ is over 16 times deeper than the out-of-phase grating $[\Delta\sigma_2(x,t)/\sigma_2]$. This is to be expected, as the excess qp population will most strongly influence σ_1, for frequencies below the pair-splitting frequency.

As a means of probing the laser-induced optical index grating, and hence probing the dynamics of the qp diffusion, the direct diffraction of mm waves by the grating could be measured. Our calculations reveal, however, that the grating diffraction peaks in the reflection and transmission of 357.4-GHz radiation are very weak (though perhaps just measurable) due to the very shallow penetration of mm waves into the film, which limits their interaction with the grating. We, therefore, propose enhancing this EM interaction with the superconductor's grating by exciting guided waves (GW) in a dielectric substrate. The GW's repeatedly reflect off the superconductor as they propagate parallel to the film, increasing the effective interaction length with the film. From elementary theory we have calculated the dispersion curves of fourteen transverse magnetic (TM) GW modes at 357.4 GHz in a 2-mm-thick film with a dielectic constant of $\epsilon_a = 10$ that is bound by a perfect conductor and by vacuum. The branches of the GW dispersion curve lie between the vacuum light line $\omega = ck$ and the dielectric light line $\omega = ck/\sqrt{\epsilon_a}$ and hence do not couple to vacuum modes. Coupling of incident mm waves to the GW's via the superconductor grating occurs with the same strength, i.e., same limitations, as the direct diffraction of the mm waves. Thus, we have considered coupling into the GWs with a prism coupler, represented by the semi-infinite dielectric overlayer of $\epsilon_b = 20$ depicted in Fig. 9.

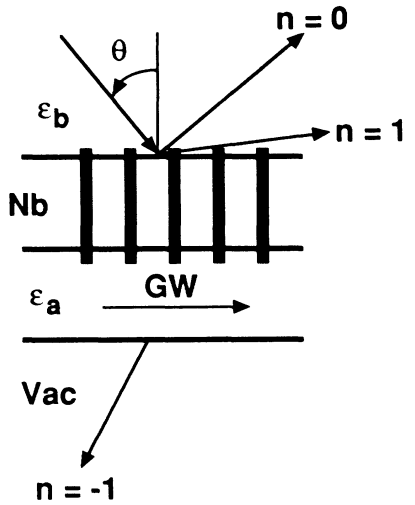

FIG. 9. Schematic of the system used to diffract mm waves from an optical index grating induced in a Nb film. The mm wave is incident on the Nb film at angle θ from a medium characterized by dielectric constant ϵ_b, representing a prism. The Nb film is on a substrate characterized by ϵ_a, which supports TM guided waves. The reflected specular beam and diffracted beam of order $n = 1$ as well as the transmitted-diffracted beam of order $n = -1$ are depicted.

The prism is a stronger coupler than the grating, strong enough to overcome the limited penetration through the film. Once the GW is excited it can then interact with the grating along its entire propagation length, out coupling through the grating diffracted orders back into the prism as well as into the lower vacuum.

To analyze the scattering of incident EM waves from the four-layer system depicted in Fig. 9, we developed an exact coupled-mode theory (based on the single-interface work of Glass and Maradudin[13]), which we plan to describe in a forthcoming publication.

A p-polarized wave incident from medium ϵ_b (the prism) onto the film at angle θ can resonantly excite a TM GW in medium ϵ_a when the component of its wave vector parallel to the film, $K_i=(\sqrt{\epsilon_b}\omega/c)\sin\theta$, equals that of the GW, K_{TM}. This GW can reradiate directly back through the prism with a reflectance angle equal to the incidence angle, or it can undergo nth-order grating diffraction and reemerge in the prism at a reflectance angle θ^n, given by $(\sqrt{\epsilon_b}\omega/c)\sin\theta^n=K_i+2\pi n/a$ (for $n=\pm1, \pm2,...$). If $|K_i+2\pi n/a|<\omega/c$, the grating can couple the GW into the vacuum, i.e., a transmitted wave of diffraction order "n" will appear (where no transmission can appear in the absence of the grating). We now present our results for diffraction from the conductivity grating depicted in Fig. 8 at the time $t=5\bar{\tau}_R$, the pulse cutoff time, when the system has nearly reached its steady-state configuration.

Figure 10 shows the intensities of (a) the reflected-diffracted wave of order $n=+1$ and of (b) the transmitted-diffracted wave of order $n=-1$ as functions of the incident angle θ (intensities relative to that of the incident wave, i.e., the grating efficiencies). The large peak in Fig. 10(a) and the peak in Fig. 10(b) are precisely identified by their position ($\theta\cong13.5°$) to correspond to the prism excitation of the TM_1 mode. For the small peak in Fig. 10(a) ($\theta\cong13.35°$), $K_i<K_{\mathrm{TM}_1}$ so that there is no direct prism coupling into the GW; however, we find that $K_i+2\pi/a=K_{\mathrm{TM}_1}$. Thus, the grating is coupling the incident wave into the GW and *then* the prism is directly out coupling it. This is still an $n=+1$ grating process, but since the grating coupling to the GW occurs first, it suffers from the same limitation as the direct grating diffraction (without a prism). In fact, this peak is similar to those obtained from direct grating coupling.

The dependence of the peak heights on the film thickness d confirms the picture just described. The direct grating coupling of an incident wave into a GW depends on the overlap of the EM field with the conductivity grating, and this overlap is limited in space to the penetration depth λ_p of the incident wave. If $\lambda_p\gg d$, then making d smaller has little effect on the coupling. When λ_p becomes comparable to d, then decreasing d begins to decrease the grating interaction. This is the behavior observed in the small $n=1$ reflectance peak. On the other hand, for prism coupling across the superconducting film into the substrate's GW's, the smaller d the stronger the prism coupling. The increase in the GW excitation with shrinking d far outweighs the small effect of d on the subsequent grating-diffracted reradiation. This effect is seen

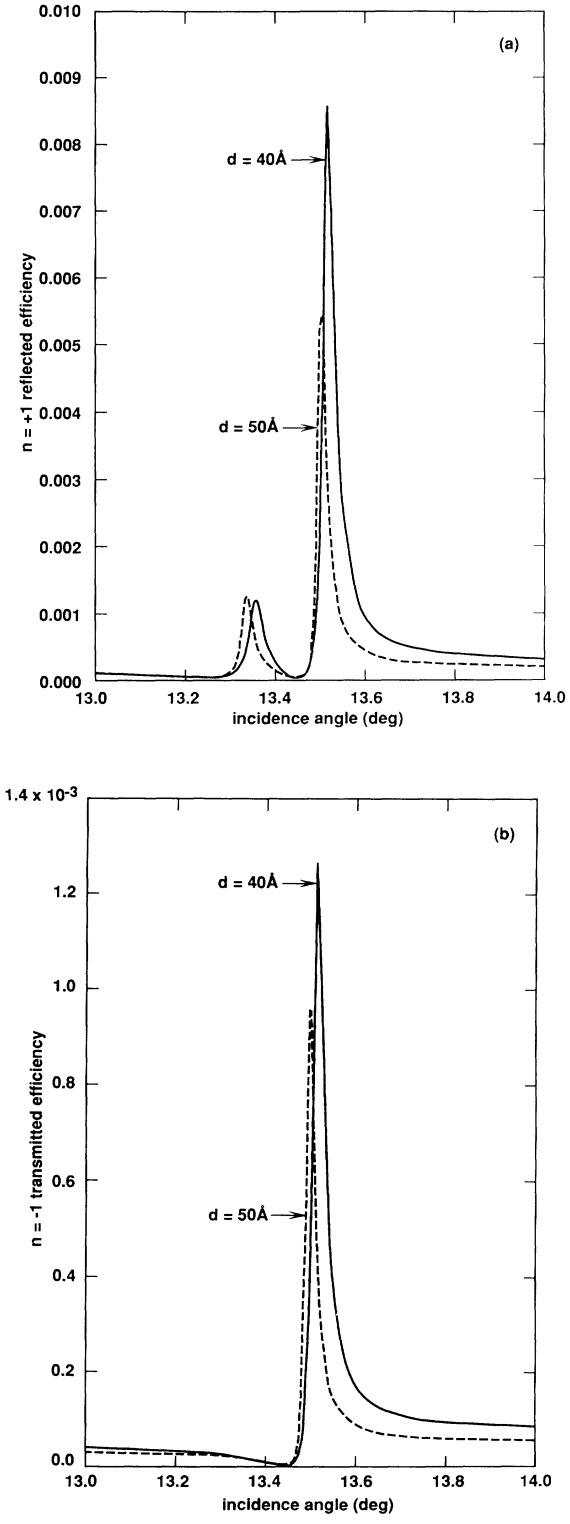

FIG. 10. The grating efficiency as a function of the angle of incidence for (a) the $n=+1$ diffracted beam in the reflected direction and for (b) the $n=-1$ grating-diffracted beam in the transmitted direction, for 357.4 GHz waves incident on the four-layer geometry depicted schematically in Fig. 9. The Nb film is of either 40- or 50-Å thickness. The optically driven conductivity grating within the Nb film is the one plotted in Fig. 8 at $t=5\bar{\tau}_R$, corresponding to the qp grating in Fig. 7.

in the increase of the large peak in Fig. 10(a) and of the peak in Fig. 10(b) as a function of decreasing d.

IV. SUMMARY AND CONCLUSIONS

We have calculated the qp spatial profiles in a thin-film superconductor in the presence of a nonuniform optical intensity field, allowing for qp diffusion. The importance of qp diffusion is clearly demonstrated by the qp structures that are predicted to form in the presence of a circular spot of optical irradiation with a Gaussian beam profile. In slow systems where phonon trapping greatly enhances the qp diffusion lengths, the qp structures may be washed out to a large extent. These diffusion effects can be determined as a function of time, within the current theoretical framework, and if correlated with real-time experiments, could yield valuable information on qp dynamics in nonequilibrium superconductors. We have also seen how, with the right choice of parameters, the qp diffusion effects can be made small enough that the induced qp structures can remain well defined while under illumination. Thus the idea of optically patterning a superconductor, for practical application, as is done in the field of nonlinear optics, is plausible. Furthermore, the time scales for the formation and dissipation of the qp structures is a short one ($\approx$ nanoseconds), so that rapid switching is feasible. The qp diffusion, which helps to erase the qp pattern after the illuminating beam is switched off, actually aids us by speeding up the recovery time.

These conclusions, formed by studying the Gaussian spot, led us to investigate the formation of optically induced gratings in superconducting thin films. Our calculations indicate that well-defined qp grating structures can be induced, under reasonable laser powers and moderate temperatures ($T=0.5T_c$), even in the presence of qp diffusion. The qp structures in turn produce conductivity gratings (phase and amplitude gratings) at microwave frequencies. In particular, the calculated mm wave grating-diffraction efficiencies, ranging from 0.1 to 0.9%, should be detectable. By monitoring the time evolution of the GW resonance peaks, one might directly monitor the qp dynamics of an optically driven nonequilibrium superconductor. This technique could provide a method of exploring qp creation, diffusion, and recombination, providing additional information on the time and length scales involved in qp dynamics in conventional superconductors. We stress, particularly, the importance of the spatial information (involving qp diffusion in a nonequilibrium superconductor) that might be thus obtained. For example, the diffusion coefficients $D_{\mathrm{qp\,(ph)}}$ might be determined. By contrast, past experiments, from the early work of Testardi[14] to the recent work of Johnson *et al.*,[15] have measured the time response of superconductors under uniform illumination.

In well-studied systems where the fundamental physics, at least of the equilibrium state, is thought to be understood, experiments could serve as a check on the present theory—especially on the limits of validity of the T^* formalism. In new and less well-understood superconducting systems, added information on the time scales and length scales might supplement existing knowledge on the basic interactions (e.g., pairing).

Furthermore, this work demonstrates that creating optical index gratings in superconductors may offer a way of performing the functions of nonlinear optics, at mm wavelengths, while exploiting some of the unique properties of superconductors (e.g., low losses and high speed, with lower power requirements than in semiconductors due to the smaller gap).

ACKNOWLEDGMENT

This work was performed with support from the Independent Research and Development Program of Rockwell International Corporation.

[1]H. J. Eichler, P. Gunter, and P. W. Pohl, *Laser-Induced Dynamic Gratings* (Springer-Verlag, New York, 1986).
[2]N. E. Glass and D. Rogovin, Appl. Phys. Lett. **54**, 182 (1989).
[3]N. E. Glass and D. Rogovin, Phys. Rev. B **39**, 327 (1989).
[4]*Nonequilibrium Superconductivity,* edited by D. N. Langenberg and A. I. Larkin (North-Holland, New York, 1986).
[5]*Nonequilibrium Superconductivity, Phonons, and Kapitza Boundaries,* Vol. 65 of *NATO Advanced Study Institute, Series B: Physics,* edited by Kenneth G. Gray (Plenum, New York, 1981).
[6]A. Rothwarf and B. N. Taylor, Phys. Rev. Lett. **19**, 27 (1967).
[7]W. H. Parker, Phys. Rev. B **12**, 3667 (1975).
[8]Jhy-Jiun Chang, Warren Y. Lai, and D. J. Scalapino, Phys. Rev. B **20**, 2739 (1979).
[9]See, for example, review by A.-M.S. Tremblay, in *Nonequilibrium Superconductivity, Phonons, and Kapitza Boundaries* (Ref. 4), pp. 289–340, or I. Iguchi and H. Konno, Phys. Rev. B **28**, 4040 (1983).
[10]D. C. Mattis and J. Bardeen, Phys. Rev. **111**, 412 (1958).
[11]Jhy-Jiun Chang and D. J. Scalapino, J. Low Temp. Phys. **3**, 1 (1978).
[12]S. B. Kaplan, C. C. Chi, D. N. Langenberg, J. J. Chang, S. Jafarey, and D. J. Scalapino, Phys. Rev. B **14**, 4854 (1976).
[13]N. E. Glass and A. A. Maradudin, Phys. Rev. B **29**, 1840 (1984).
[14]L. R. Testardi, Phys. Rev. B **4**, 2189 (1971).
[15]Mark Johnson, N. Bluzer, M. Reyzer, T. H. Geballe, S. R. Greenfield, John J. Stankus, M. D. Fayer, and C. Herring, IEEE Trans. Mag. **MAG-27**, 1523 (1991).